Proceedings of the Institution of Mechanical Engineers, Part I: Journal of Systems and Control Engineering
http://pii.sagepub.com/

Piezoelectrically actuated hydraulic valve design for high bandwidth and flow performance

D T Branson, F C Wang, D N Johnston, D G Tilley, C R Bowen and P S Keogh

Proceedings of the Institution of Mechanical Engineers, Part I: Journal of Systems and Control Engineering 2011 225: 345
DOI: 10.1177/09596518JSCE1037

Piezoelectrically actuated hydraulic valve design for high bandwidth and flow performance

D T Branson, F C Wang, D N Johnston, D G Tilley, C R Bowen, and **P S Keogh***
Department of Mechanical Engineering, University of Bath, Bath, UK

The manuscript was received on 9 March 2010 and was accepted after revision for publication on 19 August 2010.

DOI: 10.1177/09596518JSCE1037

Abstract: The performance of hydraulically actuated machine systems could be improved with the use of valves that have high bandwidth and high flowrates under low pressure drops. Although high flowrates can be achieved using very large spool strokes and/or diameters, the overall bandwidth of the valve will be reduced. Research has therefore been undertaken on a prototype valve design incorporating the Hörbiger plate principle, which utilizes multiple metering edges to allow high flowrates to be obtained at low pressure drops and small poppet displacements. The valve is directly activated using a piezoelectric actuator to achieve a fast dynamic response. Valve performance is assessed using a mathematical model that includes the piezoelectric actuator and power amplifier, the supply flow, fluid squeeze forces, end stop response, and valve mechanical components. The steady state relationship between valve flow, force and pressure drop, and the fluid inertance, were determined using computational fluid dynamics software. The simulation model has been validated using test data obtained from experimental tests undertaken on a prototype valve. Good agreement is obtained between the predicted and measured results and it is shown that the valve is capable of opening or closing fully in less than 1.5 ms, and can pass a flow of 65 l/min at a pressure drop of 20 bar.

Keywords: piezoelectric actuation, hydraulic valve design, high bandwidth, Hörbiger plates

1 INTRODUCTION

Future machine systems would benefit significantly if their operational capabilities and precision under hydraulic actuation could be increased. Although hydraulically actuated systems offer high power densities and are capable of delivering large forces over long strokes (e.g. 3 MN over 3 m to open the Gateshead Millennium Bridge [**1**]), they have a relatively low bandwidth, typically between 1 and 100 Hz. Piezoelectric actuators, on the other hand, have relatively high force capacity and bandwidth (>1 kHz), but their stroke lengths are several orders of magnitude lower than hydraulic actuators. An ideal actuator would integrate high force levels, high bandwidth, and full stroke range, with the precision associated with a piezoelectric system. The ultimate requirement is to be able to achieve dynamic positioning of an actuator over a range of stroke lengths. A necessary condition for this is the ability to precisely regulate the valve flow characteristics over a range of pressure differences and input frequencies.

Previous approaches to the technical challenge for high-performance hydraulic systems involved the use of valves having large spool strokes and diameters to achieve high flowrates [**2**]. However, this hinders the dynamic response due to increased mass and displacement. Recently, research has focused on the integration of piezoelectric actuators into hydraulic valves to increase dynamic performance [**3**, **4**]. Since the maximum free displacement of a piezoelectric actuator is generally small due to the relatively low maximum strain that is achievable (~ 0.1 per cent) [**5**], the displacement is typically enhanced by mechanical amplification [**6–9**]. The mechanical linkage must be very stiff to withstand the resulting forces, where the effects of compliance in the linkage and mass of the moving parts are

**Corresponding author: Department of Mechanical Engineering, University of Bath, Faculty of Engineering and Design, Claverton Down, Bath BA2 7AY, UK.*
email: P.S.Keogh@bath.ac.uk

amplified by the lever ratio, thus greatly reducing the actuation bandwidth. Alternative valve designs have used a two-stage arrangement, with a piezoelectric actuator operating a pilot stage valve, which then actuates the main stage valve hydraulically [**10–13**], but this introduces delays due to fluid compressibility and flow restrictions in the pilot lines.

To reduce spool stroke length and increase flow path area, Winkler and Scheidl [**14**] proposed the use of multiple metering edges using the Hörbiger plate valve principle that is commonly used in compressor applications [**15–17**]. The advantage of using Hörbiger plates is that the spool stroke required can be greatly reduced, thus improving dynamic valve response. The use of this principle in combination with a hydraulically piloted on/off valve allowed flowrates up to 100 l/min for a 5 bar pressure drop, and opening times down to 3.5 ms [**14**]. To improve valve response further, the Hörbiger plates could be integrated directly with a high-bandwidth piezoelectric multi-layer actuator. However, because the seat valve for the Winkler–Scheidl design has to be displaced by 0.6 mm, direct piezoelectric actuation of the components is not practical. In principle, this problem could be overcome by increasing the number of metering edges. The Winkler–Scheidl design is also limited in that the valve is only capable of open/close performance. Direct piezoactuation of the moving parts will not only greatly increase movement speed but also allow for proportional control of the valve. Current industrial electrohydraulic servo valves and high-performance proportional valves typically have bandwidths in the range from 150 to 300 Hz [**18**, **19**]. Piezoelectric actuation should, with appropriate system design, be able to extend this into the kilohertz range.

This paper describes the design and initial testing of a prototype high-performance valve in which the Hörbiger plates are directly activated by a piezoelectric actuator. Computational fluid dynamics (CFD) simulations are used to predict the pressure/flow/force characteristics and fluid inertance parameters for the valve [**20–22**]. These results are then used in a computer simulation model that allows the performance of the valve, piezoelectric actuator, and power amplifier to be determined. Simulated and experimental results for the dynamic response of the prototype valve are then compared for validation purposes.

2 PRINCIPLES OF THE HÖRBIGER PLATE

The Hörbiger plate is based on the use of annular grooves in two opposing valve plates to form multiple metering edges that form large flow path areas at relatively small plate separations [**14–17**]. When the plates are separated, fluid passes through the grooves formed in the plates as shown diagrammatically in Fig. 1. The use of multiple grooves greatly increases the overall flow area compared with traditional poppet and spool configurations. Hence, for a given pressure drop there is the potential to achieve higher flowrates. This is an important feature since conventional valves require high pressure drops to achieve high flowrates at small displacements.

Using the Hörbiger concept, the flowrate can be controlled simply by adjusting the distance between the two plates. Typically, the flow will be expected to saturate at plate separations above one half of the groove width [**14**]: that is when the combined circumferential flow areas adjacent to a groove due to separation exceed the radial flow area of the groove. The smaller the groove width the smaller the required plate separation and the faster the achievable switching time of the valve. However, this feature is limited by manufacturing processes, oil contamination, and fluid friction effects if the groove dimensions are too small.

3 VALVE DESIGN OVERVIEW

Figure 2 shows a simple schematic of the proposed valve. It is shown as a 'normally open' valve with a multi-layered piezoelectric lead zirconate titanate actuator directly moving the upper plate. The moving plate interfaces with a stationary lower plate when the piezoelectric actuator is fully extended. Plate separation occurs as the applied voltage is reduced and the actuator displacement is decreased.

For the final prototype design, a commercially available piezoelectric actuator with a free displacement range of $0 \leqslant x_p \leqslant X_p$ was selected, with

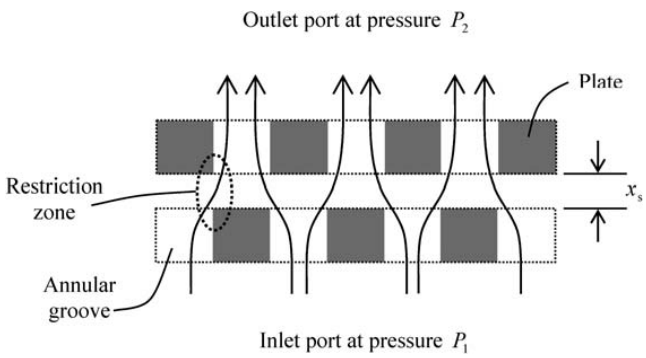

Fig. 1 Schematic radial cross-section of flow paths through multiple annular grooves under plate separation x_s

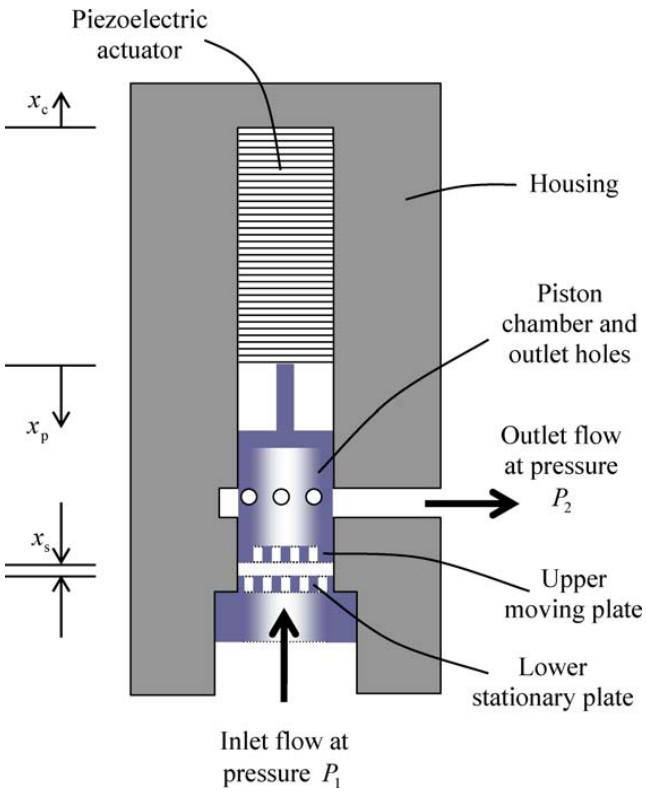

Fig. 2 Schematic cross-section of the prototype piezoelectrically actuated valve, shown with plates separated. Under actuation, the upper plate displaces by x_p to reduce the separation

$X_p = 68\,\mu m$. The force generated by the piezoelectric actuator is dependent on its displacement, with maximum stall force occurring at zero displacement and zero force produced at maximum displacement. The linearized equation for the actuator force, excluding dynamic effects, is given by

$$F_a = k_V V - k_x x_p \tag{1}$$

where V is the applied voltage, x_p is the extension of the actuator, k_x is the actuator stiffness, and k_V is a force/voltage coefficient. Experimental testing indicated that the housing of the prototype valve inevitably deflected by an amount x_c due to the reaction force acting on the upper plate. Hence, the plate separation distance, $x_s = X_p - x_p + x_c$, will generally be greater than the ideal undeflected valve. It was therefore necessary to apply a practical limit of 43 μm to the maximum plate separation distance when there is no pressure in the system, i.e. with no fluid pressure the actuator would need to displace by 43 μm to close the valve. This ensured that there was sufficient actuator force and displacement to keep the flow paths closed under the desired operating pressure of 8 bar. Adjustments to the valve could be made to limit its displacement to smaller values, allowing for operation at higher pressures. However, this will mean a reduction in experimental steady state flowrates.

The plates were designed with flat faces and six annular grooves on the lower stationary plate and five grooves on the upper moving plate (Fig. 3). To supply flow through the annular grooves, holes were positioned in the opposing surface of the plate (Fig. 3(b)). These allow fluid to pass through the grooves, while maintaining structural strength and rigidity of the plates. The upper plate is part of a hollow piston with annular grooves on the lower face. The grooves connect to the chamber inside the piston via multiple radial holes that allow the fluid to pass to the outlet port. The grooves in both plates are 1 mm wide and the supply flow enters from the bottom of the valve and exits from the side, as shown by the flow line in Fig. 2. CFD simulations indicated that the flow through these holes had a negligible effect on the overall flow/pressure characteristics (less than 0.3 bar pressure drop for a flowrate of 40 l/min).

The piezoelectric actuator used in the valve had a 12.5 kN stall force at zero displacement, and was

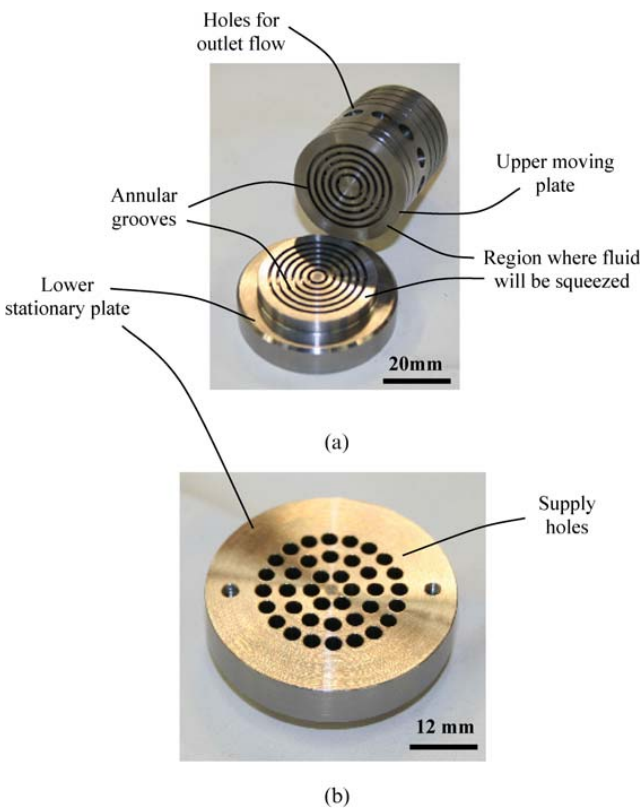

Fig. 3 (a) Image of Hörbiger plates and (b) image of the underside of the lower stationary plate showing supply holes

preloaded by 2 kN. To power the actuator an amplifier was chosen capable of supplying up to 2 A at 1000 V with a −3 dB reduction in voltage supply at approximately 550 Hz.

4 INERTANCE ANALYSIS

Fluid inertance relates the rate of change of flowrate to a given pressure drop. If fluid compressibility effects are ignored, the pressure drop across a component can be represented through resistive and inertance terms under dynamic conditions as

$$\begin{aligned}\Delta P &= P_1 - P_2 \\ &= \Delta P_{ss}(q_v, x_s) + L(x_s)\frac{dq_v}{dt}\end{aligned} \tag{2}$$

where ΔP is the dynamic pressure drop across the plates, P_1 and P_2 are the inlet and outlet pressures, respectively (Fig. 2), and L is an inertance term. The steady state pressure drop, ΔP_{ss}, is a function of the steady flowrate, q_v, and also the plate separation, x_s.

Johnston [**21**] describes a method that allows the fluid inertance of hydraulic components to be determined by configuring a CFD solver with a constrained form of the Navier–Stokes equations. It is based on the premise that the fluid acceleration field in response to a pressure change is similar to the velocity field for steady flow through a porous medium of the same geometry. The isotropic porous medium has a suitably high resistivity, R, leading to the following equation for the fluid inertance

$$L = \frac{\Delta P}{q_v}\frac{\rho\kappa}{\mu} \tag{3}$$

where ρ is the fluid density, μ is the dynamic viscosity, and κ is the permeability associated with the porous medium.

4.1 CFD simulations

To determine the steady state pressure/flow characteristic for the valve and the inertance, L, CFD simulations were undertaken at different plate separation distances using ANSYS CFX [**23**]. At small plate separations a fine mesh was needed to model the flow accurately through regions of greater restriction. Grid density and practical simulation time limitations led to the choice of a 12° circumferential section of the plate faces as a solution domain (Fig. 4). A variable density mesh was used in the model with higher grid densities in regions where flow would be restricted so that simulation accuracy was maintained. Although Fig. 4 has limited resolution in the vicinity of the plate restriction zones, Fig. 5 is included to show the finer grid detail in a single zone. Simulations were undertaken for plate separation distances $0 \leqslant x_s \leqslant 50\,\mu m$ and a pressure drop across the plates in the range $0 \leqslant \Delta P \leqslant 150$ bar. The groove overlap was set to 0 μm, and the properties of a standard mineral-oil-based hydraulic fluid

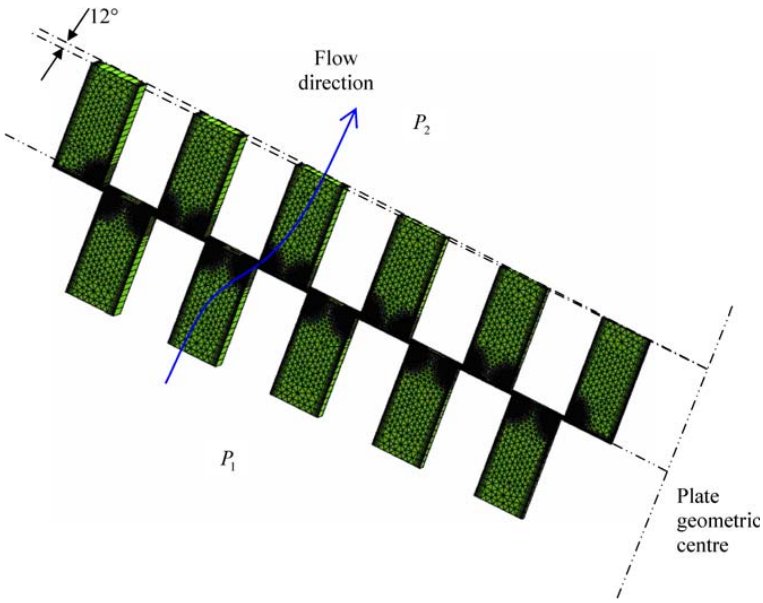

Fig. 4 Example mesh for a 12° section of the annular groove fluid solution domain used in ANSYS CFX simulations. The mesh density was adjusted for each plate separation

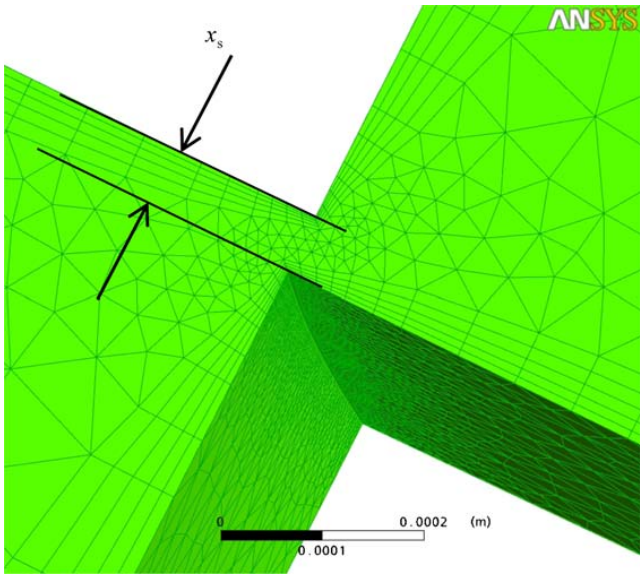

Fig. 5 Expanded view showing the variation in mesh density across the flow restriction region

were used. Figure 6 shows the predicted variation in the inertance with plate separation.

5 VALVE SIMULATION MODEL

The model is based on dynamic equations for the valve partitioned into sub-models for the power amplifier, the combined piezoelectric actuator and upper moving plate, the fluid squeeze between the plates, and the valve characteristics. The inputs are the desired piezoactuator position, x_i, and inlet and outlet pressures P_1 and P_2. Parameter values used in the simulation are given in Table 1.

5.1 Sub-model 1: piezoelectric amplifier/actuator

In general, the actuator capacitance will limit the build-up of the applied voltage. Assuming the amplifier has an infinite bandwidth, the time taken to reach the maximum voltage can be calculated according to [**24**]

$$\Delta t = C_p \frac{\Delta V}{i_{max}} = 9 \times 10^{-7} \left(\frac{1000}{2} \right) = 0.4 \text{ ms} \tag{4}$$

where Δt is the time period, C_p is the capacitance of the actuator, ΔV is the voltage change across the actuator, and i_{max} is the maximum current that can be supplied by the amplifier. However, equation (4) does not take into account the frequency limitations in the power amplifier. Hence, the actuation time of equation (4) is not practically achievable.

An improved model was obtained by representing the dynamic response of the power amplifier and actuator as a second-order system. The output voltage V can then be found by integrating the following equation with respect to time

$$\ddot{V} = -2\zeta_a \omega_{na} \dot{V} - \omega_{na}^2 V + \omega_{na}^2 V_i \tag{5}$$

where ζ_a and ω_{na} are the amplifier/actuator damping ratio and natural frequency inferred from the

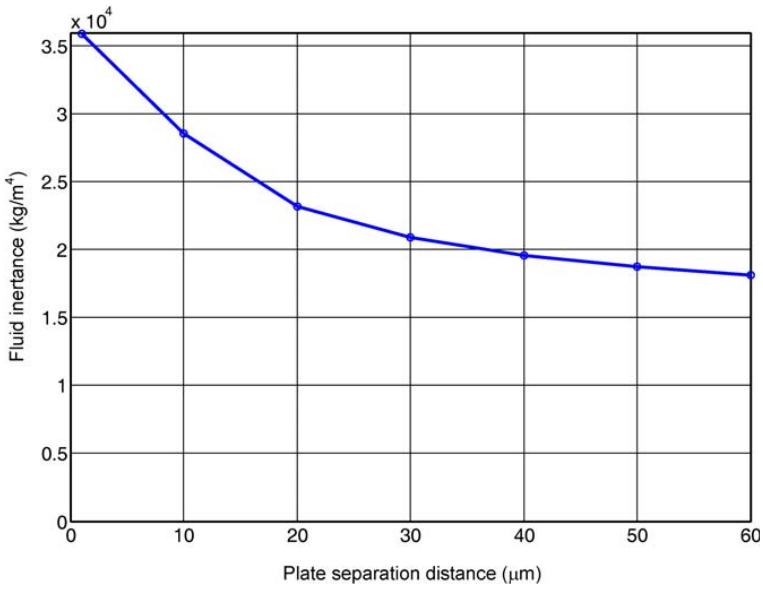

Fig. 6 Fluid inertance as a function of plate separation distance, x_s

manufacturer's data sheets. The desired amplifier voltage is related to the desired actuator position according to $V_i = V_{max}(x_i/X_p)$.

5.2 Sub-model 2: actuator and upper moving plate

The static representation of equation (1) may now be used for the dynamic response of the combined actuator and upper moving plate in the form of a second-order differential equation for the displacement, x_p

$$m_{xp}\ddot{x}_p + c_x\dot{x}_p + k_x x_p = F_V - F_E \tag{6}$$

where m_{xp} is the combined effective mass of the actuator and the upper moving plate

$$m_{xp} = m_x + \frac{1}{3}m_p \tag{7}$$

where m_x is the plate mass and m_p is the mass of the piezoactuator. The factor of one-third in equation (7) accounts for the proportional extension of the actuator from the fixed end. The equivalent viscous damping coefficient c_x is associated with the upper moving plate and actuator. Without fluid coupling, the plate/actuator system represented by equation (6) is lightly damped and a proportion of critical damping at around 0.125 was considered appropriate. The voltage-dependent force is given by

$$F_V = k_V V \tag{8}$$

The remaining external force, F_E, is the superposition of the end stop force, F_e, the fluid squeeze force between the valve plates, F_s, the force acting on the upper moving plate due to flow in the separation region, F_v, and the force, F_2, on the upper moving plate due to pressure P_2

$$F_E = F_e + F_s + F_v + F_2 \tag{9}$$

The size and stack construction of the piezoelectric actuator dictate that the upper moving plate would make contact with the lower stationary plate at distances less than the maximum possible value for x_p. It was therefore necessary to include upper and lower movement end stops on the actuator to model contact. An end stop can be modelled in terms of a stiff spring, k_e, together with an equivalent viscous damping term, c_e, to prevent numerically induced high-frequency oscillations that can reduce simulation efficiency. The end stop force F_e is then expressible as

$$F_e = \begin{cases} 0, & x_s > X_s \\ -c_e\dot{x}_s - k_e x_s, & x_s < X_s \end{cases} \tag{10}$$

where X_s is a threshold separation below which contact is considered to occur.

5.3 Sub-model 3: fluid squeeze force

As the plate separation distance decreases there is a contained region of fluid at the outer edge of the plate that will be squeezed. Although this region is relatively small, the force created by fluid squeeze could be significant in terms of the closing speed and separation distance. The Reynolds equation for thrust bearings [**25**] was used to evaluate the squeeze force as follows

$$F_s = \begin{cases} \pi(R_o^2 - R_i^2)P_1, & \dot{x}_s \geq 0 \\ \pi(R_o^2 - R_i^2)P_1 + \dfrac{3\pi\mu}{x_s^3}\dot{x}_s\Lambda, & \dot{x}_s < 0 \end{cases} \tag{11}$$

where

$$\Lambda = \left[\frac{(R_o^2 - R_i^2)^2}{4} + \frac{R_o^2(R_o^2 - R_i^2)}{2} - R_o^4 \ln\left(\frac{R_o}{R_i}\right)\right] \tag{12}$$

and R_i and R_o are the inner and outer radii to the fluid squeeze region as shown in Fig. 7.

In equation (11), the constant force when $\dot{x}_s \geq 0$ is associated with fluid cavitation when the plate separation is increasing. It can be seen in equation (11) that as x_s decreases to zero F_s becomes infinite, which would cause numerical simulation issues. The force expression included in equation (11) was therefore limited using

$$F_s = \frac{x_s}{X_s}\left[\pi(R_o^2 - R_i^2)P_1 + \frac{3\pi\mu}{X_s^3}\dot{x}_s\Lambda\right] \tag{13}$$

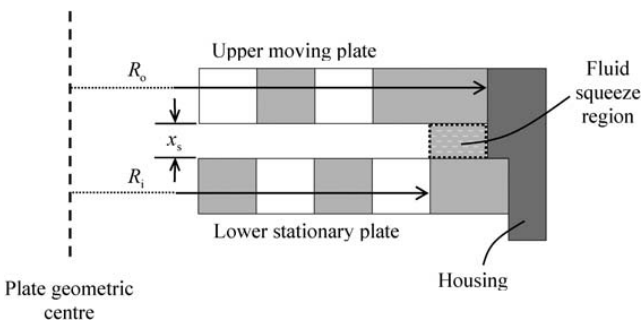

Fig. 7 Schematic of the fluid squeeze region

when $x_s < X_s$ and $\dot{x}_s < 0$, where X_s is the selected threshold distance. This threshold may be based on the size of asperities at the interface.

5.4 Sub-model 4: valve characteristic

The valve characteristic sub-model can be separated into further sub-models for the force acting on the upper moving plate, compliance in the housing, and the determination of valve flow based on plate separation distance, pressure drop, and supply flow.

5.4.1 Force acting on upper plate

The force acting on the upper moving plate due to flow in the separation region, F_v, was found as part of the steady state ANSYS CFX simulations undertaken to determine the inertance and pressure/flow characteristics. This force arises from P_1 acting against the plate, and the flow forces due to pressure changes caused by the motion of fluid through the flow restriction regions. The force due to P_1 acting on the solid centre part of the upper plate was also included in the final calculations.

The variations of F_v are shown in Fig. 8, where there is a general increase as a function of the pressure drop across the valve. However, the force also decreases as x_s increases. This is due to the increase in fluid flow force as the flow through the restriction regions increases. Figure 8 was converted to a look-up table for simulation purposes.

An additional force, F_2, was included to account for the effect of P_2 on the outlet side of the upper moving plate

$$F_2 = P_2 A_2 \tag{14}$$

where A_2 is the effective area of the upper moving plate.

5.4.2 Housing compliance

Experimental testing showed that the measured deflections of the housing were significant. The force applied to the housing will depend on the inlet and outlet pressures. By considering the areas associated with the piston of Fig. 2, the steady force transmitted to the piezoactuator, and hence the housing, is expressible in terms of the pressure difference, ΔP, and the residual outlet pressure, P_2. In the experimental phase the inlet pressure was varied up to 150 bar while the outlet pressure was limited to be less than 5 bar. Therefore, to include the effect of housing compliance deformation, x_c, tests were undertaken on the prototype valve to determine the additional separation of the plates as a function of the steady state pressure drop across the valve (Fig. 9). A second-order polynomial curve with zero-offset was then used to obtain the following empirical relationship between x_c and the pressure drop

$$x_c = 0.03621(\Delta P)^2 + 1.75498\Delta P \tag{15}$$

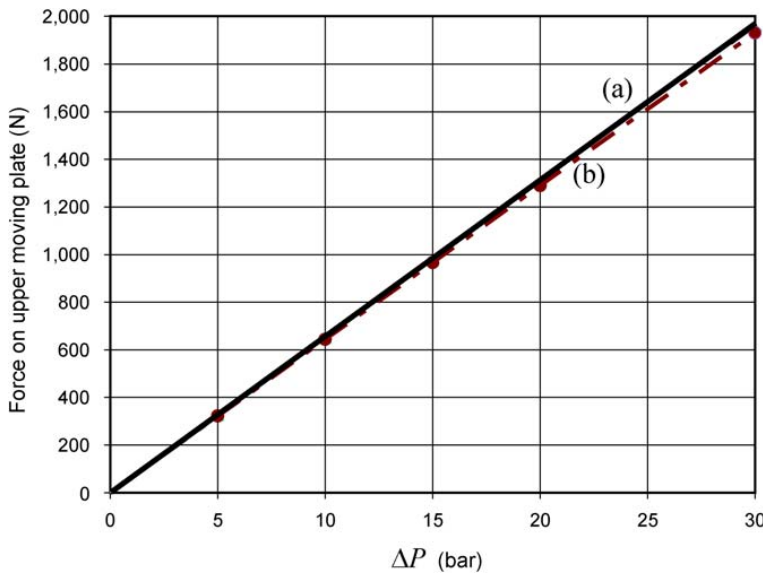

Fig. 8 Steady state force acting on the upper plate as a function of plate separation distance and pressure drop: plot (a) 10 μm separation, 0 μm overlap, and plot (b) 40 μm separation, 0 μm overlap

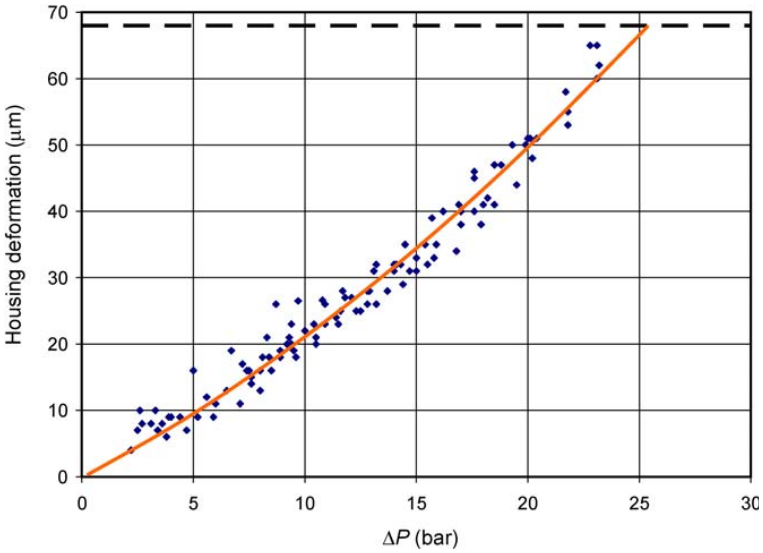

Fig. 9 Housing deformation, x_c, as a function of pressure drop across the valve. The experimental results (♦) have been curve fitted (—) up to the maximum possible 68 μm

where ΔP is in bar and x_c is in micrometres. The relationship given by equation (15) is valid for low outlet pressures. The actual plate separation distance is then related to the actuator extension by

$$x_s = X_p - x_p + x_c \tag{16}$$

As it was not possible to determine dynamic housing compliance effects, equation (16) was used for both steady state and dynamic conditions. Additional analysis (e.g. finite element) of the housing dynamics could be included to account for any high-frequency dynamic modes, but this was considered to be outside the scope of the current work.

5.4.3 *Flow through the valve*

To solve for the flow response of the valve, equation (2) is first rearranged as

$$\dot{q}_v = \frac{1}{L}(P_1 - P_2 - \Delta P_{ss}) \tag{17}$$

The valve flowrate, q_v, is obtained by numerically integrating equation (17) with respect to time. The rates of change of the valve inlet pressure, $\dot{P}_1$, and outlet pressure, $\dot{P}_2$, can be found from

$$\dot{P}_1 = \frac{\beta}{V_1}(Q_s - q_v) \tag{18}$$

$$\dot{P}_2 = \frac{\beta}{V_2}(q_v - Q_o) \tag{19}$$

where Q_o is the flow out of the valve to tank, β is the bulk modulus of the fluid, and V_1 and V_2 are the volumes of fluid on the inlet and outlet sides of the valve, respectively.

The supply flow is determined in a separate sub-model as

$$Q_s = \begin{cases} Q_{smax}, & P_1 \leqslant P_r \\ Q_{smax} - Q_r, & P_1 > P_r \end{cases} \tag{20}$$

where Q_{smax} is the maximum available supply flow from the supply, P_r is the relief valve pressure setting, and Q_r is the relief valve flow to tank when P_1 exceeds P_r, as given by

$$Q_r = K_r(P_1 - P_r) \tag{21}$$

where K_r is the flow/pressure gradient for the relief valve. Since the outlet is connected directly to the tank, P_r is constant and Q_o is assumed to be equal to q_v.

The procedure is to solve equations (17) to (21) for given values of β, V_1, V_2, x_s, and Q_s along with data in a look-up table for ΔP_{ss} as a function of q_v and x_s, and L as a function of x_s. Multiple CFD simulations and flow measurements were undertaken by varying the pressure difference across the plates from 0 to 150 bar for plate separations at 0, 10, 20, 30, and 40 μm. The look-up table was derived from the simulation data.

6 EXPERIMENTAL AND SIMULATION RESULTS

Experimental tests were undertaken to evaluate both the steady state and dynamic response character-

istics of the prototype valve. Piezo-resistive pressure sensors were located at the inlet and outlet to the valve and a turbine flow meter located at the outlet. The steady state plate separation was measured directly using a position sensor located on the upper moving plate. Although the sensor is capable of measurements up to 7 kHz, due to space limitations it was not possible to directly attach it to the upper moving plate, and contact was simply maintained by the sensor return spring. Hence, contact may have been lost momentarily during rapid movements. In addition, there was significant measurement noise, which was filtered out for the steady state results. For these reasons, the position sensor was not suitable for dynamic measurements. Piezoelectric actuator displacements were determined using strain gauge sensors integrated into the actuator. A real-time interface system was used for measurement and to control the displacement of the actuator.

6.1 Steady state flow

Figure 10 shows a comparison between the simulated and experimental steady state flow characteristics for the valve as a function of plate separation and pressure drop across the valve for simulations using a 0 μm groove overlap. The 69 l/min limit of the hydraulic fluid supply is also indicated in Fig. 10. Both results show that flow increases as the pressure drop and plate separation distance increase.

6.2 Dynamic plate separation measurement

The piezoelectric actuator strain gauge enabled high-bandwidth measurement of the actuator extension. This is related to the separation of the plates, but differs because the separation of the plates is affected strongly by the compliance of the valve housing. Since it was not possible to measure dynamic plate separation in a reliable manner, the dynamic separation was inferred using the steady state plate separation position sensor and piezoactuator strain gauge displacement

$$x_{ds} = \frac{X_{ss}}{X_{pt}}\left(X_p - x_p\right) + x_{s0} \tag{22}$$

where x_{ds} is the inferred dynamic separation distance between the plates, X_{ss} is the total steady state separation distance over the test, X_{pt} is the total actuator displacement, x_p is obtained from the strain gauge measurement, X_p is the maximum unrestricted displacement of the actuator (68 μm), and x_{s0} is the initial steady state separation of the plates when the piezoactuator is fully excited (1000 V).

6.2.1 *Open/close performance*

In the current configuration the valve will crack open at pressures above 8 bar. Because the lowest system pressure achievable is 5 bar, tests were completed at 15 bar to show the dynamic effect of increasing pressure without excessive housing compliance. Figure 11

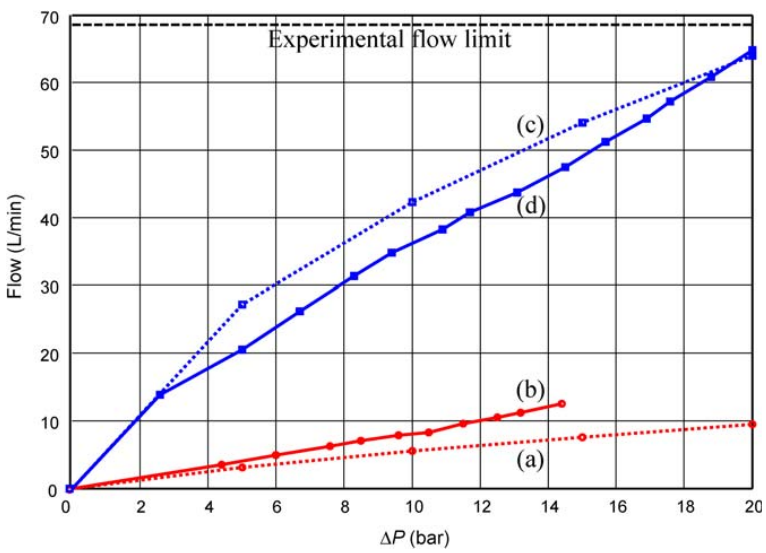

Fig. 10 Steady state flow characteristics for the valve as a function of plate separation and pressure drop across the valve: plot (a) simulated with 10 μm separation, plot (b) experimental with 10 μm separation, plot (c) simulated with 40 μm separation, and plot (d) experimental with 40 μm separation

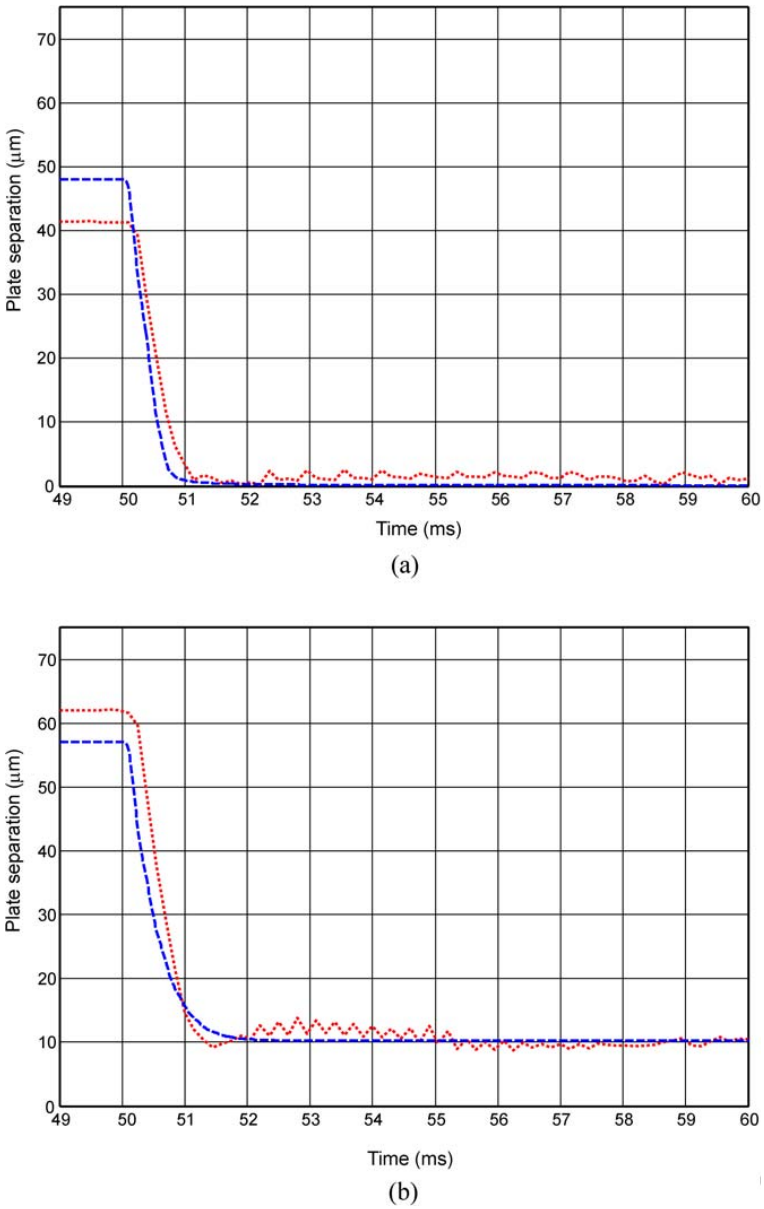

Fig. 11 Plate separation, x_{ds}, as a function of time for various ΔP across the valve: (a) $\Delta P = 5$ bar and (b) $\Delta P = 15$ bar. The actuator was commanded to extend (0 V to 1000 V input) at time = 50 ms thus closing the valve. Experimental separation (▪▪▪▪), simulated separation (----)

shows x_{ds} for a step command to fully close the valve at pressure drops of 5 and 15 bar. This was accomplished by switching the voltage supplied to the actuator from 0 V to 1000 V at 50 ms. It can be seen that the time to achieve minimum plate separation for the valve increases from approximately 1 ms at $\Delta P = 5$ bar to 1.1 ms at $\Delta P = 15$ bar. This is due to the increased pressure forces on the moving plate resisting valve closure. At $\Delta P = 15$ bar it can also be seen that the valve does not completely close due to housing compliance. The small difference in final position is due to sensor error. Differences in final steady state displacement are associated with the simulation model, which is set up to give the same flow for a given pressure drop as that found in the experimental valve. Product literature indicated that the sensors were accurate to within 0.5 μm, though instrumentation bias/noise increased this uncertainty to ± 5 μm. Hence, there was a significant variation in the position sensor output with respect to a system that is only moving by 60 μm. However, there was no recorded flow when the valve was nominally closed and the outlet pressure drop to the tank was zero. The assumption

under these measured conditions was that the valve was closed.

Differences between the predicted and measured dynamic performance are due mainly to the second-order form of equation (5) used to model the actuator/power amplifier. Also, the dynamics of the fluid in the supply and return lines have not been included in the model. Experimental testing has indicated that the amplifier may not behave as a second-order system at higher frequencies, and further testing is needed to improve the model accuracy. Differences could also be due to friction, damping, and fluid compression around the upper moving plate, which are not accounted for in the model.

Figure 12 shows the plate separation that follows a voltage step command to open the valve (1000 V to 0 V at 50 ms). It can be seen that increasing ΔP across the valve increases the rate at which the valve opens. However, due to compliance in the housing the

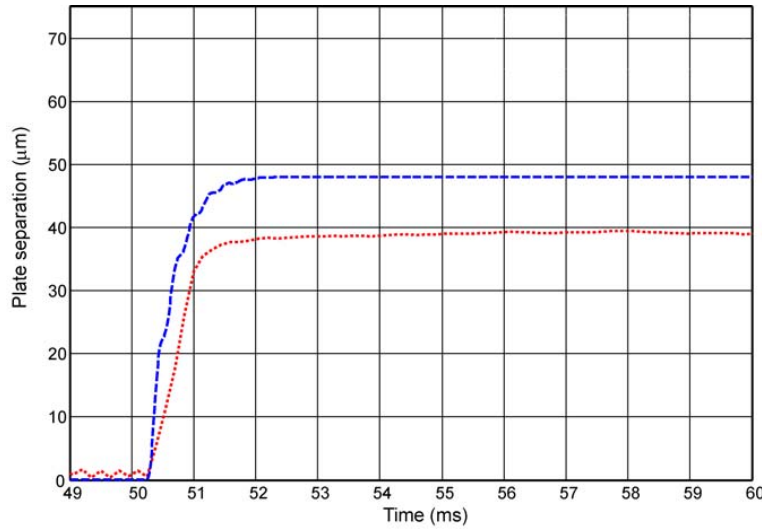

(a) $\Delta P = 5$ bar

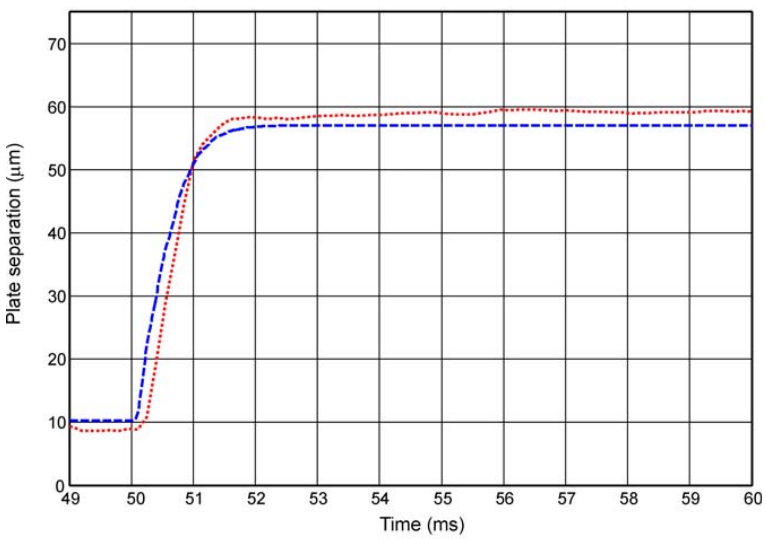

(b) $\Delta P = 15$ bar

Fig. 12 Plate separation, x_{ds}, as a function of time for various ΔP across the valve: (a) $\Delta P = 5$ bar, and (b) $\Delta P = 15$ bar. The actuator was commanded to extend (1000 V to 0 V input) at time = 50 ms thus opening the valve. Experimental separation (▪▪▪▪), simulated separation (----)

maximum displacement of the upper moving plate is also increased, and the overall time to open is approximately the same at 1.5 ms. This increase in opening rate is due to the fact that the supply pressure forces assisted the motion of the moving plate. It can also be seen that the valve does not start from the fully closed position at $\Delta P = 15$ bar due to housing compliance. The difference in steady state performance is due to the flow/pressure characteristics used in the simulation. The results of Fig. 12 also show creep displacement occurring in the experimental valve. Creep can occur in a piezoelectric actuator due to a delayed response to domain switching [**26**, **27**]. However, because creep displacements are relatively small, they were not included in the simulation.

6.3 Bandwidth performance

Additional experimental testing was undertaken to determine valve bandwidth performance. To do this a sine wave demand signal at different amplitudes, superimposed on a bias signal of +500 V, was output from the power amplifier. The supply pressure was set to 11 bar to ensure that the valve would only just close at the maximum voltage. This was undertaken to allow the greatest possible motion, while ensuring that the upper moving plate would not repeatedly impact the lower stationary plate at higher frequencies, thus potentially damaging the piezoelectric actuator.

The resulting piezoelectric actuator displacement, x_p, was measured and the results compared as a function of input frequency and amplitude (Fig. 13). It can be seen that increasing the amplitude of the input signal reduces the -3 dB valve response frequency from over 2 kHz with $V = 500 \pm 140$ V (28 per cent of maximum) to 420 Hz with $V = 500 \pm 425$ V (85 per cent of maximum). Further testing showed that the decrease in valve motion at higher frequencies is strongly influenced by the piezoactuator amplifier limitations. In Fig. 13 the observed magnitudes decrease at a faster rate than would be predicted by the second-order model of equation (5). This highlights the need for a more accurate high-frequency amplifier model in future work. Nonetheless, the performance of the valve still exceeds that of current industrial electrohydraulic servo valves and high-performance proportional valves, which typically achieve maximum performance in the range 150–300 Hz for 90 per cent of maximum spool displacement [**18**, **19**].

7 CONCLUSIONS

A novel valve design that incorporates the Hörbiger plate principle has been assessed. For high bandwidths the valve is directly operated by a piezoelectric stack actuator, and it is configured to be normally open. A dynamic mathematical model is presented, which includes the electrical power supply, piezoactuator, mechanical valve components, fluid squeeze forces, and forces acting on the components due to pressure and flow. The model includes steady state flow and fluid inertance properties determined from CFD studies.

The simulation model was used to evaluate the steady state and dynamic response characteristics of

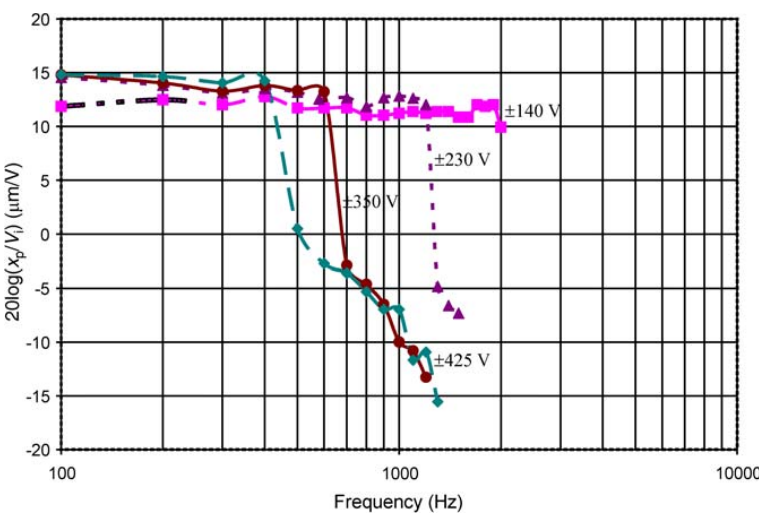

Fig. 13 Bandwidth comparison: variation of amplitude of x_p in response to V_i as a sine wave input command with bias +500 V and increasing amplitude as annotated

Table 1 System parameter values

Description	Parameter	Value
Effective area of the upper plate	A_2	$5.79\times10^{-4}\,\mathrm{m}^2$
Damping associated with upper plate and actuator	c_x	1800 Ns/m
End stop damping	c_e	1×10^{8} Ns/m
Actuator stiffness	k_x	2.1×10^{8} N/m
End stop stiffness	k_e	1×10^{22} N/m
Piezoactuator force/voltage coefficient	k_v	12.5 N/V
Flow/pressure gradient coefficient for relief valve	K_r	1×10^{6} l/s/bar
Mass associated with piezoelectric actuator deflection	m_x	0.171 kg
Mass of the upper plate	m_p	0.221 kg
Inlet pressure	P_1	0–150 bar
Outlet pressure	P_2	0–5 bar
Maximum voltage output of the amplifier	V_{max}	1000 V
Volume of fluid on the inlet side of the valve	V_1	$1.3\times10^{-5}\,\mathrm{m}^3$
Volume of fluid on the outlet side of the valve	V_2	$3.6\times10^{-5}\,\mathrm{m}^3$
Inner radius to the fluid squeeze region	R_i	0.0137 m
Outer radius to the fluid squeeze region	R_o	0.0165 m
Maximum unrestricted displacement of actuator	X_p	6.8×10^{-5} m
Actuator displacement to end stop	X_{pe}	4.3×10^{-5} m
Squeeze film threshold	X_s	1×10^{-8} m
Fluid bulk modulus	β	1.5×10^{9} Pa
Fluid density	ρ	864 kg/m^3
Fluid viscosity (dynamic)	μ	0.0342 PAs
Amplifier natural frequency	ω_{na}	3454 rad/s
Amplifier damping ratio	ζ_a	1

the valve. These indicate that large flowrates can be obtained at very small plate separation distances. For example, 66.5 l/min could be achieved at a pressure drop of 20 bar and 40 μm plate separation. Decreasing the plate separation distance or pressure drop across the plates reduces the steady state flowrate through the valve.

The dynamic response of the valve to a step command was also evaluated. It was found that the time to close the valve increased from approximately 1 ms at 5 bar pressure drop to 1.1 ms at 15 bar. The time to open the valve was approximately 1.5 ms regardless of the pressure drop, although the rate of opening and final plate separation distances increased with pressure drop. The Winkler–Scheidl valve did allow for higher flowrates of up to 100 l/min at $\Delta P = 5$ bar. However, the dynamic performance for their valve was slower, where the fastest total valve opening time was 3.5 ms, and the fastest closing time 3.2 ms. The Winkler–Scheidl valve is also limited to open/close performance whereas the valve developed for this paper can achieve proportional control.

The bandwidth performance of the valve was also investigated experimentally with full actuator displacement up to 425 Hz for input voltage amplitudes up to 85 per cent of maximum, and no drop off in piezoactuator displacement up to 2 kHz for input voltages less than 28 per cent of maximum. This exceeds the performance of industrial electrohydraulic servo valves and high-performance proportional valves, which typically operate in the range 150–300 Hz.

The resulting valve concept will be developed further and integrated into future systems to improve overall hydraulic actuation system performance. The work reported in the paper relates to the open-loop response characteristics of the valve. When integrated into a complete system, closed-loop control would be the expectation. A number of control strategies may be implemented that could utilize the dynamic range of the valve. In future work, the modelled open-loop characteristics may also be used to assess closed-loop system stability and performance optimization.

ACKNOWLEDGEMENT

The authors wish to thank the Engineering and Physical Sciences Research Council of the UK for funding this project through grant EP/D060478/1.

REFERENCES

1 **Tilley, D. G., Keogh, P. S., Mutch, K., Robotham, M., Curran, P.,** and **Mehrkar-Asl, S.** Making the eye blink – modelling the operation of the Gateshead Millennium Bridge. *Proc. IMechE, Part C: J. Mechanical Engineering Science*, 2003, **217**, 735–758. DOI: 10.1243/09544060/3767764390.

2 **Scheidl, R., Steiner, B., Winkler, B.,** and **Mikota, G.** Basic problems in fast hydraulic switching valve technology. In Proceedings of the Sixth International

Conference on *Fluid power transmission and control*, Zhejiang University, Hangzhou, China, 5–8 April 2005, pp. 53–57 (International Academic Publishers Ltd, Hong Kong).

3 **Wong, A. P., Bullough, W. A., Chin, S. B.,** and **Chua, Y. S.** Performance of the piezo-poppet valve. Part 1. *Proc. IMechE, Part I: J. Systems and Control Engineering*, 2006, **220**, 439–451. DOI: 10.1243/09596518JSCE139.

4 **Wong, A. P., Bullough, W. A., Chin, S. B.,** and **Chua, Y. S.** Performance of the piezo-poppet valve. Part 2. *Proc. IMechE, Part I: J. Systems and Control Engineering*, 2006, **220**, 453–471. DOI: 10.1243/09596518JSCE140.

5 **deVries, J. W. C.** Functional behavior of ceramic multilayer actuators with inactive parts. *Sens. Actuators*, 1999, **72**, 251–255.

6 **Brader, J. S.** and **Rocheleau, D. N.** Development of a piezoelectrically-controlled hydraulic actuator for a camless engine. Part 1: system design. *Proc. IMechE, Part D: J. Automobile Engineering*, 2004, **218**, 817–822. DOI: 10.1243/0954407041581084.

7 **Brader, J. S.** and **Rocheleau, D. N.** Development of a piezoelectrically-controlled hydraulic actuator for a camless engine. Part 2: system modelling. *Proc. IMechE, Part D: J. Automobile Engineering*, 2004, **218**, 823–830. DOI: 10.1243/0954407041581129.

8 **Lindler, J. E.** and **Anderson, E. H.** Piezoelectric direct drive servovalve. SPIE Conference on Industrial and Commercial Applications of Smart Structures and Technologies, San Diego, California, 2002.

9 **Bart, H. U.** *Piezoelectric fuel injector valve*, 4101 076, USA, 1978.

10 **Bang, Y.-B., Joo, C.-S., Lee, K.-I., Hur, J.-W.,** and **Lim, W.-K.** Development of a two-stage high speed electrohydraulic servovalve system using stack-type piezoelectric elements. In Proceedings of the 2003 IEEE/ASME International Conference on *Advanced intelligent mechatronics*, Kobe, Japan, 20–24 July 2003 vol. 1, pp. 131–136 (IEEE, New York).

11 **Reichert, M.** Development of a piezo-driven pilot stage for highly dynamic hydraulic valves. In Proceedings of the Fifth International Conference on *Fluid power*, Aachen, Germany, 20–22 March 2006, vol. 2, pp. 127–137 (University of Aachen, Germany).

12 **Xiaoping, O., Tilley, D. G., Keogh, P. S., Yang, H., Johnston, D. N., Bowen, C. R.,** and **Hopkins, P.** Piezoelectric actuators for screw-in cartridge valves. The IEEE/ASME International Conference on Advanced Intelligent Mechatronics, Xi'an, China, 2008.

13 **Igashira, T., Sakakibara, Y., Watanabe, K.,** and **Murate, N.** *Piezoelectric flow control valve*, 4728 074, USA, 1988.

14 **Winkler, B.** and **Scheidl, R.** Development of a fast seat type switching valve for big flow rates. In Proceedings of the Tenth Scandinavian International Conference on *Fluid power*, Tampere, Finland, 21–23 May 2007, pp. 137–146. (Tampere University of Technology, Finland).

15 **Rogler, F. W.** and **Hörbiger, H.** *An improved automatic valve*, 190 608 487, UK, 1907.

16 **Hörbiger, A.** *Annular automatic valve*, 2127 688, USA, 1938.

17 **Kehler, K.** *Automatic annular valve*, 2186 489, USA, 1940.

18 Parker Hydraulics. Direct operated proportional DC valves – series D1FP, catalogue, HY14-2550/US, A61–A72, Parker Hydraulics, 2010.

19 MOOG Industrial Controls Division. Electrohydraulic valves. A technical look, product literature, CDL6566 Rev D, 500-170 302, MOOG Industrial Controls Division, 2010.

20 **Lau, K. K., Edge, K. A.,** and **Johnston, D. N.** Impedance characteristics of hydraulic orifices. *Proc. IMechE, Part I: J. Systems and Control Engineering*, 1995, **209**, 241–253.

21 **Johnston, D. N.** Prediction of fluid inertance in nonuniform passageways. *Trans. ASME, J. Fluids Engng*, 2006, **128**, 266–275.

22 **Boyd, L. J., Roberts, A. P., Collet, A. P. S., Johnston, D. N., Tilley, D. G.,** and **Edge, K. A.** Prediction of hydraulic inertance using acoustic measurements and CFD modelling. ASME International Mechanical Engineering Congress and Exposition, Chicago, Illinois, 5–10 November 2006.

23 ANSYS Inc. ANSYS CFX reference guide – release 11.0, ANSYS Inc., 2006.

24 Physik Instruments. The world of micro- and nanopositioning catalogue, Physik Instruments, 2005–2006.

25 **Robinson, C. L.** and **Cameron, A.** Studies in hydrodynamic thrust bearings, I. Theory considering thermal and elastic distortions. *Phil. Trans. R. Soc. Lond., Series A: Math. Phys. Sci.*, 1975, **278**, 351–366.

26 **Jung, H., Shim, J. Y.,** and **Gweon, D.** Tracking control of piezoelectric actuators. *Nanotechnology*, 2001, **12**, 14–20.

27 **Giddings, P., Bowen, C. R., Butler, R.,** and **Kim, H. A.** Characterisation of actuation properties of piezoelectric bi-stable carbon-fibre laminates. *Compos., Part A: Appl. Sci. Mfg*, 2008, **39**, 697–703.

APPENDIX

Notation

A_2	effective area of the upper plate
c_e	end stop damping
c_x	damping associated with upper plate and actuator
C_p	piezoactuator capacitance
F_e	force due to the end stop
F_s	force due to fluid squeeze between the valve plates
F_E	external force acting on the upper plate

F_v	force acting on the upper plate due to flow in the separation region
F_V	voltage-induced force
F_2	pressure-induced force on the upper plate
i_{max}	maximum current supplied by the amplifier
k_e	end stop stiffness
k_V	piezoactuator force/voltage coefficient
k_x	piezoactuator stiffness
K_r	flow/pressure gradient coefficient for relief valve
L	inertance plate
m_p	mass of the upper plate
m_x	mass associated with piezoelectric actuator deflection
m_{xp}	combined effective mass of the piezoactuator and upper moving plate
P_r	relief valve pressure setting
$P_{1,2}$	inlet, outlet pressure
ΔP	pressure drop across the plates
ΔP_{ss}	steady state pressure drop
q_v	dynamic component of valve flow-rate
Q_o	flow out of the valve to tank
Q_r	flowrate to tank
Q_s	supply flowrate
Q_{smax}	maximum supply flowrate
Q_v	steady valve flowrate
$R_{i,o}$	inner, outer radius to the fluid squeeze region
Δt	minimum time to attain maximum voltage across piezoactuator
V	amplifier voltage output
ΔV	voltage change across actuator
V_i	desired actuator voltage
V_{max}	maximum voltage output of the amplifier
$V_{1,2}$	volume of fluid on the inlet, outlet side of the valve
x_c	housing deformation
x_{ds}	inferred dynamic separation distance between the plates
x_i	desired actuator displacement
x_p	piezoactuator displacement
x_s	plate separation distance
x_{s0}	displacement of the plate when the actuator is fully excited
X_p	maximum unrestricted displacement of piezoactuator
X_{pe}	piezoactuator displacement to end stop
X_{pt}	total actuator displacement
X_s	squeeze film threshold
X_{ss}	total steady state separation distance over the dynamic test
β	bulk modulus of the fluid
ζ_a	amplifier damping ratio
κ	permeability of nominal porous medium
μ	fluid viscosity
ρ	fluid density
ω_{na}	amplifier natural frequency